Datasheet for 200-301-379

# RFP Antibody

## Overview

| | |
|---|---|
| **Description:** | Anti-RFP (MOUSE) Monoclonal Antibody - 200-301-379 |
| **Item No.:** | 200-301-379 |
| **Size:** | 100 µg |
| **Applications:** | ELISA, WB, FISH, IF, IHC, Multiplex |
| **Reactivity:** | RFP, mCherry, rRFP |
| **Host Species:** | Mouse |

## Product Details

| | |
|---|---|
| **Background:** | Antibodies to RFP (Discosoma spp.) are intended for use in immunological assays including ELISA, Western blotting, immunohistochemistry, and flow cytometry. RFP Proteins are useful markers for imagining protein localization, monitoring physiological processes, and detecting transgenic expression. Rockland's anti-RFP antibody can be used to detect native RFP and RFP variants. |
| **Synonyms:** | mouse anti-RFP Antibody, DsRed, rDsRed, Discosoma sp. Red Fluorescent Protein, Red fluorescent protein drFP583 |
| **Host Species:** | Mouse |
| **Clonality:** | Monoclonal |
| **Clone ID:** | 8E5.G7 |
| **Format:** | IgG2a |

## Target Details

| | |
|---|---|
| **Gene Name:** | DsRed |
| **Reactivity:** | RFP, mCherry, rRFP |
| **Immunogen Type:** | Recombinant Protein |
| **Immunogen:** | The immunogen is a Red Fluorescent Protein (RFP) fusion protein corresponding to the full-length amino acid sequence (234aa) derived from the mushroom anemone Discosoma. |

| | |
|---|---|
| **Purity/Specificity:** | Anti-RFP Monoclonal Antibody was purified from concentrated tissue culture supernate by Protein A chromatography. Expect reactivity against RFP and its variants: mCherry, tdTomato, mBanana, mOrange, mPlum, mOrange and mStrawberry. |
| **Relevant Links:** | • UniProtKB - Q9U6Y8 |

## Application Details

| | |
|---|---|
| **Tested Applications:** | ELISA, WB |
| **Suggested Applications:** | FISH, IF, IHC, Multiplex (Based on references) |
| **Application Note:** | Monoclonal anti-RFP is designed to detect RFP and its variants. This antibody has been tested by ELISA and Western blot, and is suitable for use in FISH, IF, IHC, and multiplex assays based on published references. This antibody can be used to detect RFP by ELISA (sandwich or capture) for the direct binding of antigen. Optimal titers for applications should be determined by the researcher. |
| **Assay Dilutions:** | All assays should be optimized by the user. Recommended dilutions (if any) may be listed below. |
| **ELISA:** | 1:75,000 - 1:150,000 |
| **FC:** | User Optimized |
| **IF:** | User Optimized |
| **IP:** | User Optimized |
| **WB:** | 1:1,000 - 1:10,000 |

## Formulation

| | |
|---|---|
| **Physical State:** | Liquid (sterile filtered) |
| **Concentration:** | 1.004 by UV absorbance at 280 nm |
| **Buffer:** | 0.02 M Potassium Phosphate, 0.15 M Sodium Chloride, pH 7.2 |
| **Preservative:** | 0.01% (w/v) Sodium Azide |
| **Stabilizer:** | None |

## Shipping & Handling

| | |
|---|---|
| **Shipping Condition:** | Dry Ice |

| | |
|---|---|
| **Storage Condition:** | Store anti-RFP at -20° C prior to opening. Aliquot contents and freeze at -20° C or below for extended storage. Avoid cycles of freezing and thawing. Centrifuge product if not completely clear after standing at room temperature. This product is stable for several weeks at 4° C as an undiluted liquid. Dilute only prior to immediate use. |
| **Expiration:** | Expiration date is one (1) year from date of receipt. |

## Images

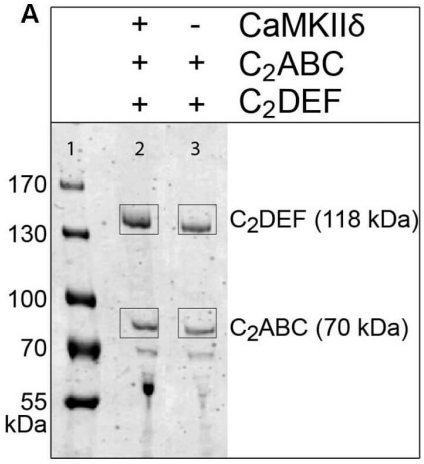


**Western Blot**
Otoferlin is phosphorylated by CaMKIIδ in vitro. (A) Otoferlin fragments C2ABC (aa 1–616 in NP_001093865, 70 kDa) and C2DEF (aa 908–1932, 118 kDa), were expressed in E. coli and subjected to an in vitro phosphorylation assay with CaMKIIδ and Ca2+/calmodulin. Reactions were stopped after 5 min of incubation and proteins were run on a Coomassie gel. Note the slight shift in mass of the fragments between experiment (lane 2) and control without kinase (lane 3). Coomassie stained bands corresponding to otoferlin C2DEF and C2ABC were cut off the gel and processed for mass spectrometric analysis of otoferlin phosphorylation (Supplementary Figure S2). (B) Three independent experiments as in (A) revealed 10 serine/threonines in otoferlin that were reproducibly phosphorylated by CaMKIIδ. The putative otoferlin domain topology (in mouse isoform 1; NP_001093865) predicts six C2 domains (C2A to C2F; purple), a coiled-coiled domain (orange), a FerB domain (yellow), and a transmembrane domain (TM) (dark gray). Five of the phosphorylation sites are located in C2 domains. Figure provided by CiteAb.
Source: Front Synaptic Neurosci, Figure 6. PMID: 29046633.

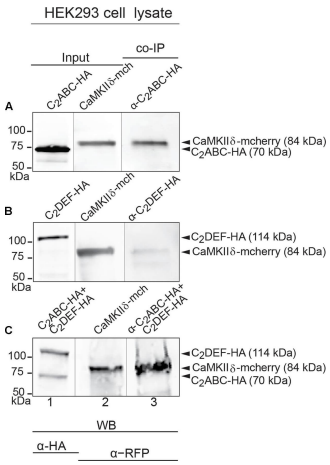


## Western Blot

Immunoprecipitation and western blot show interaction of otoferlin with CaMKIIδ. (A–C) Two HA-tagged mouse otoferlin fragments, C2ABC (aa 1–632 in NP_001093865; 70 kDa) and C2DEF (aa 933–1920; 114 kDa) were co-transfected with mcherry-tagged mouse CaMKIIδ into HEK293 cells. Transfections were performed either with otoferlin C2ABC and CaMKIIδ (A, Input Lane 1 and 2), otoferlin C2DEF and CaMKIIδ (B, Input Lane 1 and 2) or in the presence of both C2ABC and C2DEF fragments and CaMKIIδ (C, Input Lane 1 and 2). Co-immunoprecipitations of C2ABC-HA and C2DEF-HA were conducted from HEK293 cell lysates using anti-HA antibodies. CaMKIIδ-mcherry was detected in the eluate using an anti-RFP (red fluorescent protein) antibody (A–C, Lane 3), indicating that CaMKIIδ co-precipitated with recombinant otoferlin fragments. Figure provided by CiteAb. Source: Front Synaptic Neurosci, Figure 5. PMID: 29046633.

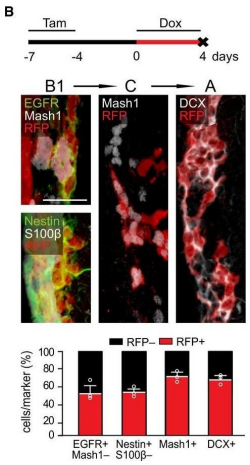


## Immunohistochemistry

Transgenic model and effects of acute 4D overexpression on NSC and progenitors of the SVZ. B. From top to bottom: experimental design of 4D induction, fluorescence pictures of the SVZ of a 4D+ mouse and quantification of the proportion of RFP− (black) and RFP+ (red) progenitors among B1, C, and A cells identified with markers as indicated. Data information: Mean ± SEM; *P < 0.05 and **P < 0.01 calculated by unpaired Student's t-test; N = 3 mice, n > 423 cells for each quantification. Scale bar = 50 µm.
Figure provided by CiteAb. Source: EMBO J, Fig 1. PMID: 30643018.

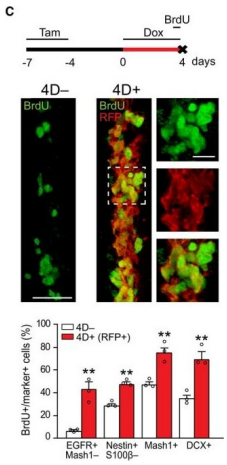


## Immunohistochemistry

Transgenic model and effects of acute 4D overexpression on NSC and progenitors of the SVZ.
C. From top to bottom: experimental design, fluorescence pictures of the SVZ of a 4D− (left) and 4D+ (right and insets magnified) mice, and quantification of the proportion of BrdU+ among B1, C, and A cells (identified as in B). Note that in 4D+ mice quantification was restricted to the RFP+ subpopulation (red bars).
Data information: Mean ± SEM; *P < 0.05 and **P < 0.01 calculated by unpaired Student's t-test; N = 3 mice, n > 423 cells for each quantification. Scale bar = 50 µm or 20 µm (inset in C).
Figure provided by CiteAb. Source: EMBO J, Fig 1. PMID: 30643018.

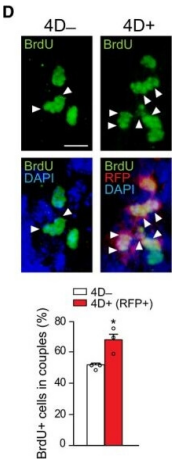


**Immunohistochemistry**
Chronic effect of 4D overexpression on NSC and OB neurogenesis. A. Experimental design used to assess the chronic effect of a transient 4D induction with BrdU and EdU given during Dox administration or 1 h before sacrifice, respectively. B–E. From top to bottom: fluorescence pictures of the SVZ (B–D) or OB (E) and absolute number (B, C, and E) or proportions (C–E) of cells in 4D− (white bars) or 4D+ (black or red bars for all or RFP+ cells, respectively) mice scored positive for various markers as indicated. Insets in (C) are magnified (right) with arrowheads pointing label-retaining NSC (white) or astrocytes (empty). Arrowheads in (D) point cell doublets (among RFP+ protein-retaining cells in 4D+). (E) GL, glomerular; EPL, external plexiform; MCL, mitral cell and GCL, granule cell layers.Data information: (B–E) Mean ± SEM; *P < 0.05, **P < 0.01 assessed by unpaired Student's t-test (bar graphs) or Fisher's exact test (pie graphs); N = 3 mice, n > 285 cells for each quantification. Scale bars = 50 µm (B, C, and E) and 20 µm (D and insets in C). Figure provided by CiteAb. Source: EMBO J, Fig 2. PMID: 30643018.

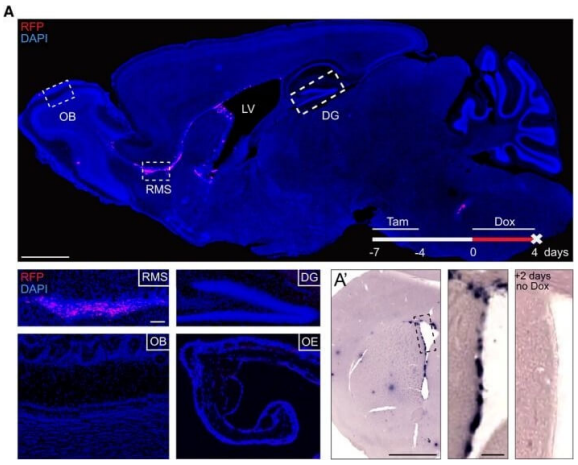


**Immunohistochemistry**
Characterization of the transgenic model and effect of 4D on the RMS.
A. Fluorescence image of a sagittal section of a 4D+ brain after a 4-day treatment with doxycycline showing RFP signal confined to the SVZ and RMS (nuclei counterstained with DAPI; blue). Insets show representative images of specific brain regions (as indicated) and the olfactory epithelium. A'. Phase contrast picture of the SVZ upon in situ hybridization against mRNA for RFP in a 4D+ brain treated as in (A) and sacrificed immediately after (left) or 2 days after (right) doxycycline administration.
(A) OB, olfactory bulb; RMS, rostral migratory stream; LV, lateral ventricle; DG, dentate gyrus; OE, olfactory epithelium. (A–C) Tam, tamoxifen; Dox, doxycycline. Scale bars = 500µm (A top, A'), 100 (insets A and A'). Figure provided by CiteAb. Source: EMBO J, Fig EV1. PMID: 30643018.

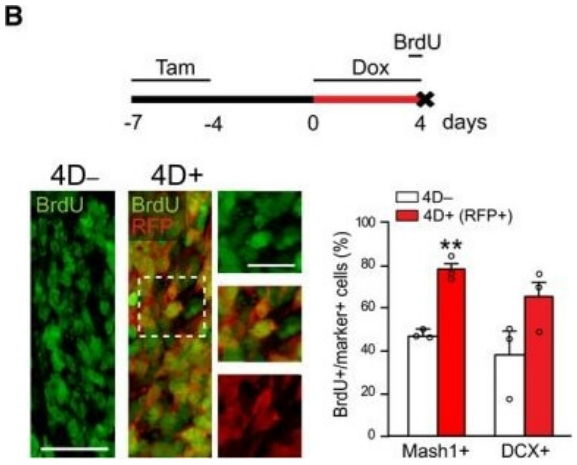


**Immunohistochemistry**
Characterization of the transgenic model and effect of 4D on the RMS.
B, C. Experimental design (top), fluorescence pictures (left with magnified insets), and quantifications (right) of BrdU incorporation in the RMS (B) or SVZ (C). (B) shows the proportion of BrdU in C (Mash1+) and A (DCX+) cells in 4D− (white) and 4D+ (red; among RFP+) mice. (C) shows the proportion of RFP− (black) and RFP+ (red) among BrdU+ cells of 4D+ mice. (A) OB, olfactory bulb; RMS, rostral migratory stream; LV, lateral ventricle; DG, dentate gyrus; OE, olfactory epithelium. (A–C) Tam, tamoxifen; Dox, doxycycline. (B, C) Mean ± SEM; **P < 0.01; unpaired Student's t-test; N = 3 mice and n > 1,100 cells. Scale bars = 500 (A top, A'), 100 (insets A and A'), 50 (B and C), and 20 (insets B and C) µm. Figure provided by CiteAb. Source: EMBO J, Fig EV1. PMID: 30643018.

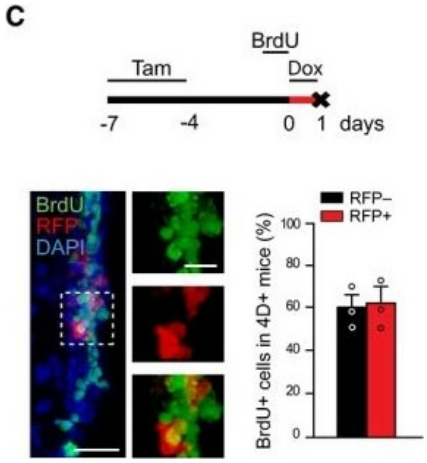


**Immunohistochemistry**
Characterization of the transgenic model and effect of 4D on the RMS.
B, C. Experimental design (top), fluorescence pictures (left with magnified insets), and quantifications (right) of BrdU incorporation in the RMS (B) or SVZ (C). (B) shows the proportion of BrdU in C (Mash1+) and A (DCX+) cells in 4D− (white) and 4D+ (red; among RFP+) mice. (C) shows the proportion of RFP− (black) and RFP+ (red) among BrdU+ cells of 4D+ mice. (A) OB, olfactory bulb; RMS, rostral migratory stream; LV, lateral ventricle; DG, dentate gyrus; OE, olfactory epithelium. (A–C) Tam, tamoxifen; Dox, doxycycline. (B, C) Mean ± SEM; **P < 0.01; unpaired Student's t-test; N = 3 mice and n > 1,100 cells. Scale bars = 500 (A top, A'), 100 (insets A and A'), 50 (B and C), and 20 (insets B and C) µm. Figure provided by CiteAb. Source: EMBO J, Fig EV1. PMID: 30643018.

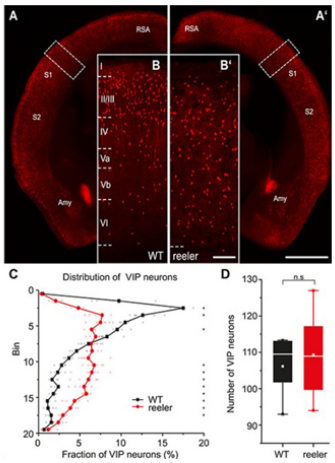


**Fluorescence in situ Hybridization (FISH)**
Distribution of VIP cells is different between WT and reeler mice. (A, A') Coronal sections at the level of the barrel cortex of WT and reeler mice in which VIP neurons are labeled with tdTomato. The areal/nuclear locations of VIP expression remained the same in WT and reeler (scale bar: 1000 µm; Amy, amygdala; RSA, retrosplenial agranular cortex; S1/S2, primary/secondary somatosensory cortex). (B, B') Close-up of barrel cortex area in WT and reeler mice (insert in A, A'). In WT, VIP neurons showed a stronger bias toward upper layers (II–IV). In reeler, VIP neurons were uniformly dispersed across the cortical thickness (scale bar: 100 µm). (C) Distribution of VIP neurons across the cortical depth. In WT, they showed a prominent peak in the upper layers. In reeler, they were fairly uniformly distributed, with few neurons close to pia and white matter (n = 5 WT mice, 6 reeler mice; 6 sections for each mouse; symbols connected by lines show average; small, transparent symbols show individual animals; asterisks highlight significantly different fractions per bin between genotypes with $P < 0.05$). (D) Number of VIP neurons counted on 40-µm-thick sections in an area of barrel cortex spanning from pia to white matter and being 1000 µm wide (n = 5 WT mice, 6 reeler mice; 6 sections each mouse; box plot: white line = median; white dot = mean). Counts were almost the same in WT and reeler ($P > 0.05$). Fig 1. PMID: 33135045

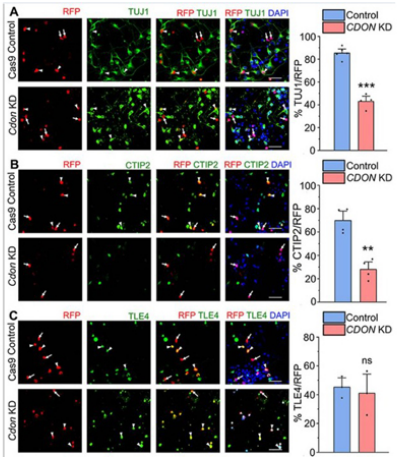


**Immunofluorescence Microscopy**
CDON regulates neurogenesis and CTIP2-expressing neurons in the neocortical progenitors. A, Neocortical progenitors of E12.5 mouse embryo transfected with the Cas9-Cdon sgRNAs vector (left panel of A–C) and immunostained with TUJ1 (green, middle panel, A), CTIP2 (green, middle panel, B), and TLE4 (green, middle panel, C) antibody. The right panel of A–C shows the bar graph with the percentage of TUJ1-positive (A), CTIP2-positive (B), and TLE4-positive (C) cells of the transfected cell populations for the Cas9 control and Cdon KD neocortical cells. Data are presented as mean ± SEM; two-tailed Student's t test; **p < 0.0, ***p < 0.001, and ns, not significant. White arrowheads indicate transfected cells which express RFP and the indicated markers of panels A–C, and white arrows show transfected cells which express RFP and do not express the indicated markers. Scale bars: A–C, 30 µm. Figure 7. Refer to S7-1 and S7-2 for more details. PMID: 39592227.

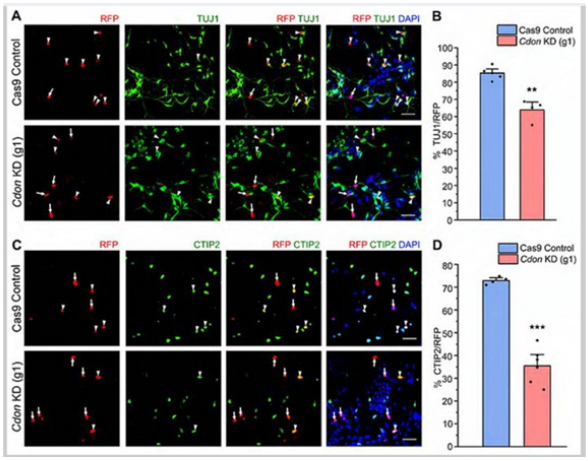


**Immunofluorescence Microscopy**
CDON knockdown using a single gRNA against Cdon results in a reduction of both total neurons and CTIP2-expressing neurons.
Neocortical progenitors of E12.5 mouse embryo transfected with a single guide RNA (Cas9-Cdon) targeting the exon 3 of Cdon. (A and C) Confocal images showing the cultured neocortical progenitors stained with anti-TUJ1 (A) and CTIP2 (C) antibodies after 5DIV. (B and D) Bar graph with the percentage of TUJ1 + ve (B) and CTIP2 + ve (D) of the total RFP transfected cell populations for the Cas9 control and Cdon KD neocortical cells. Data are presented as mean ± SEM; Two-tailed Student's t-test; ** $p < 0.01$ and *** $p < 0.001$. White arrowheads indicate transfected cells which express RFP and the indicated markers of panels A and C, and white arrows show transfected cells which express RFP and do not express the indicated markers. Scale bars for (A) and (C) are 30µm. Figure S7-2. Related to Figure 7. PMID: 39592227.

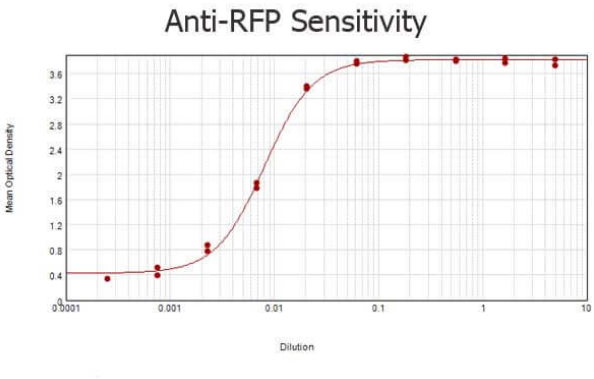


**ELISA**
ELISA results of purified Mouse anti-RFP Monoclonal Antibody tested against RFP (p/n 000-001-379). Each well was coated in duplicate with 1.0 µg of the antigen. The starting dilution of antibody was 5µg/ml and the X-axis represents the Log10 of a 3-fold dilution. This titration is a 4-parameter curve fit where the IC50 is defined as the titer of the antibody. Assay performed using 3% fish gel, anti-Mouse IgG Antibody Peroxidase Conjugated Secondary and TMB ELISA Peroxidase Substrate (p/n TMBE-1000).

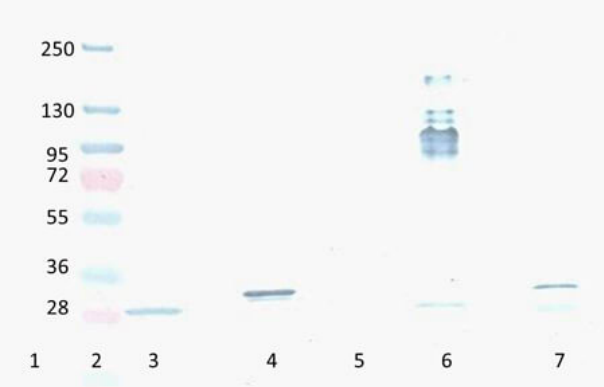


**Western Blot**
Western Blot of Mouse Anti-RFP antibody. Lane 1: YFP protein. Lane 2: Prestained Molecular Weight Marker. Lane 3: Reduced RFP control Protein. Lane 4: Reduced mCherry. Lane 5: GFP protein. Lane 6: Non-Reduced RFP control Protein. Lane 7: Non-Reduced mCherry. Load: 300ng per lane. Primary antibody: RFP antibody at 1:2000 in MB-070 for 3 hours at RT. Secondary antibody: HRP anti-Mouse secondary antibody at 1:10,000 in MB-070 for 60 min at RT. Substrate: TMBM-100 for 20 min. Predicted/Observed size: ~27 kDa.

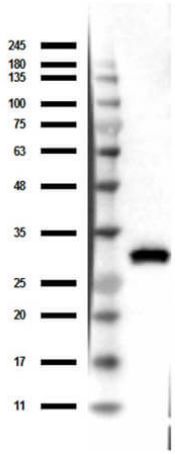


**Western Blot**
Western Blot of Mouse Anti-RFP Antibody. Lane 1: Opal Prestain Molecular weight (p/n MB-210-0500). Lane 2: 50ng of RFP. Primary Antibody: Mouse Anti-RFP at 1µg/mL overnight at 2-8°C. Secondary Antibody: Rabbit Anti-Mouse HRP (p/n 610-403-C46) at 1:40,000 for 30mins at RT. Block: BlockOut Universal blocking buffer (p/n MB-073). Expect ~27kDa.

## References


- Allgöwer, C et al. An oncogenic KRAS-driven secretome involving TNFα promotes niche preparation prior to pancreatic cancer onset. *Molecular Cancer* (2026)
- Aaltonen, A et al. Postnatal reduction of eIF4E overexpression in D1-SPNs ameliorates KCNQ channel dysfunction, hyperexcitability and ASD-like behaviours. *Cellular and Molecular Life Sciences* (2026)
- Santos TB et al. Reactivation of encoding ensembles in the prelimbic cortex supports temporal associations. *Neuropsychopharmacology.* (2024)
- Di Martino E et al. Inflammatory, metabolic, and sex-dependent gene-regulatory dynamics of microglia and macrophages in neonatal hippocampus after hypoxia-ischemia. *iScience.* (2024)
- Rangel Guerrero DK et al. Hippocampal cholecystokinin-expressing interneurons regulate temporal coding and contextual learning. *Neuron.* (2024)

- Dhanya SK et al. Histone-binding protein RBBP4 is necessary to promote neurogenesis in the developing mouse neocortical progenitors. *eNeuro.* (2024)
- Qin X et al. An oncogenic phenoscape of colonic stem cell polarization. *Cell.* (2023)
- Castillo-Azofeifa D et al. A DLG1-ARHGAP31-CDC42 axis is essential for the intestinal stem cell response to fluctuating niche Wnt signaling. *Cell Stem Cell.* (2023)
- Sun M et al. A neural pathway underlying hunger modulation of sexual receptivity in Drosophila females. *Cell Rep.* (2023)
- Meyer C et al. Tailup expression in Drosophila larval and adult cardiac valve cells. *Genesis.* (2023)
- Watanabe H et al. Purkinje Cardiomyocytes of the Adult Ventricular Conduction System Are Highly Diploid but Not Uniquely Regenerative. *J Cardiovasc Dev Dis.* (2023)
- Flanigan ME et al. Subcortical serotonin 5HT2c receptor-containing neurons sex-specifically regulate binge-like alcohol consumption, social, and arousal behaviors in mice. *Nat Commun.* (2023)
- Liu H et al. TRPC3 channel gating by lipids requires localization at the ER/PM junctions defined by STIM1. *J Cell Biol.* (2022)
- Henriques VJ et al. Astrocytes Modulate Somatostatin Interneuron Signaling in the Visual Cortex. *Cells.* (2022)
- Zhang, L et al. Nutrients and pheromones promote insulin release to inhibit courtship drive. *Science Advances* (2022)
- Vetere G et al. An inhibitory hippocampal-thalamic pathway modulates remote memory retrieval. *Nat Neurosci.* (2021)
- Wu CH et al. Homeostatic synaptic scaling establishes the specificity of an associative memory. *Curr Biol.* (2021)
- Hutton C et al. Single-cell analysis defines a pancreatic fibroblast lineage that supports anti-tumor immunity. *Cancer Cell.* (2021)
- Xiao L et al. Expression of FoxP2 in the basal ganglia regulates vocal motor sequences in the adult songbird. *Nat Commun.* (2021)
- Slupe AM et al. GABAergic neurons are susceptible to BAX-dependent apoptosis following isoflurane exposure in the neonatal period. *PLoS One.* (2021)
- Hafner G et al. Increased Callosal Connectivity in Reeler Mice Revealed by Brain-Wide Input Mapping of VIP Neurons in Barrel Cortex. *Cereb Cortex.* (2021)
- Adrados CS et al. Salamander-Eci: An optical clearing protocol for the three-dimensional exploration of regeneration. *Dev Dyn.* (2020)
- Abecassis ZA, Berceau BL, Win PH, et al. Npas1+-Nkx2.1+ Neurons Are an Integral Part of the Cortico-pallido-cortical Loop. *J Neurosci.* (2020)
- Hennes M, Lombaert N, Wahis J, Van den Haute C, Holt MG, Arckens L. Astrocytes shape the plastic response of adult cortical neurons to vision loss. *Glia* (2020)
- Guan Z, Quiñones-Frías MC, Akbergenova Y, Littleton JT. Drosophila Synaptotagmin 7 negatively regulates synaptic vesicle release and replenishment in a dosage-dependent manner. *Elife* (2020)
- Hafner G, Witte M, Guy J, et al. Mapping Brain-Wide Afferent Inputs of Parvalbumin-Expressing GABAergic Neurons in Barrel Cortex Reveals Local and Long-Range Circuit Motifs. *Cell Rep.* (2019)

- Bragado Alonso S, Reinert JK, Marichal N, et al. An increase in neural stem cells and olfactory bulb adult neurogenesis improves discrimination of highly similar odorants. *EMBO J.* (2019)
- Donovan LJ, Spencer WC, Kitt MM, et al. Lmx1b is required at multiple stages to build expansive serotonergic axon architectures. *Elife.* (2019)
- Katrancha et al. Trio Haploinsufficiency Causes Neurodevelopmental Disease-Associated Deficits. *Cell Reports* (2019)
- Singh, S et al. A new Elf5Cre ERT 2- GFP BAC transgenic mouse model for tracing Elf5 cell lineages in adult tissues. *Febs Letters* (2019)
- Vascak M, Jin X, Jacobs KM, Povlishock JT. Mild Traumatic Brain Injury Induces Structural and Functional Disconnection of Local Neocortical Inhibitory Networks via Parvalbumin Interneuron Diffuse Axonal Injury. *Cereb Cortex.* (2018)
- Rieche F, Carmine-Simmen K, Poeck B, Kretzschmar D, Strauss R. Drosophila Full-Length Amyloid Precursor Protein Is Required for Visual Working Memory and Prevents Age-Related Memory Impairment. *Curr Biol.* (2018)
- Girasole AE, Lum MY, Nathaniel D, et al. A Subpopulation of Striatal Neurons Mediates Levodopa-Induced Dyskinesia. *Neuron.* (2018)
- Sin, YY et al. Transplantation of Gene-Edited Hepatocyte-like Cells Modestly Improves Survival of Arginase-1-Deficient Mice. *Molecular Therapy. Nucleic Acids* (2018)
- Rider et al. The interactome of EBV LMP1 evaluated by proximity-based BioID approach. *Virology* (2018)
- Winkowski et al. Orbitofrontal Cortex Neurons Respond to Sound and Activate Primary Auditory Cortex Neurons. *Cerebral Cortex* (2018)
- Clarkson et al. D3 Receptors Regulate Excitability in a Unique Class of Prefrontal Pyramidal Cells. *The Journal of Neuroscience* (2017)
- Zhou et al. Subcellular Targeting of VIP Boutons in Mouse Barrel Cortex is Layer-Dependent and not Restricted to Interneurons. *Cerebral Cortex* (2017)
- Meese et al. Activity-Dependent Phosphorylation by CaMKIIδ Alters the Ca2+ Affinity of the Multi-C2-Domain Protein Otoferlin. *Frontiers in Synaptic Neuroscience* (2017)
- Hou et al. NMDA Receptors Regulate the Development of Neuronal Intrinsic Excitability through Cell-Autonomous Mechanisms. *Frontiers in Cellular Neuroscience* (2017)
- Guan et al. Eye opening differentially modulates inhibitory synaptic transmission in the developing visual cortex. *Elife* (2017)
- Bifari et al. Neurogenic Radial Glia-like Cells in Meninges Migrate and Differentiate into Functionally Integrated Neurons in the Neonatal Cortex. *Cell Stem Cell* (2017)
- Hutton SR, Otis JM, Kim EM, Lamsal Y, Stuber GD, Snider WD. ERK/MAPK Signaling Is Required for Pathway-Specific Striatal Motor Functions. *J Neurosci.* (2017)
- Dixon RE, Vivas O, Hannigan KI, Dickson EJ. Ground State Depletion Super-resolution Imaging in Mammalian Cells. *J Vis Exp.* (2017)
- Lebrigand, K et al. Comparative Genomic Analysis of Drechmeria coniospora Reveals Core and Specific Genetic Requirements for Fungal Endoparasitism of Nematodes. *PloS Genetics* (2016)

- Wu et al. Potassium and the K+/H+ Exchanger Kha1p Promote Binding of Copper to ApoFet3p Multi-copper Ferroxidase. *Journal of Biological Chemistry* (2016)
- Clancy, JW et al. Regulated delivery of molecular cargo to invasive tumour-derived microvesicles. *Nature Communications* (2015)

## Disclaimer